Ocean Sci. Discuss., 6, 95–128, 2009
www.ocean-sci-discuss.net/6/95/2009/

Ocean Science Discussions

Papers published in *Ocean Science Discussions* are under open-access review for the journal *Ocean Science*

Towards closure of regional heat budgets in the North Atlantic using Argo floats and surface flux datasets

N. C. Wells, S. A. Josey, and R. E. Hadfield

National Oceanography Centre, European Way, Southampton, SO14 3ZH, UK

Received: 20 October 2008 – Accepted: 20 October 2008 – Published: 13 January 2009

Correspondence to: N. C. Wells (n.wells@noc.soton.ac.uk)

Published by Copernicus Publications on behalf of the European Geosciences Union.

Abstract

The upper ocean heat budget (0–300 m) of the North Atlantic from 20°–60° N is investigated using data from Argo profiling floats for 1999–2005 and the NCEP/NCAR and NOC surface flux datasets. Estimates of the different terms in the budget (heat storage, advection, diffusion and surface exchange) are obtained using the methodology developed by Hadfield et al. (2007). The method includes optimal interpolation of the individual profiles to produce gridded fields with error estimates at a 10×10 degree grid box resolution. Closure of the heat budget is obtained within the error estimates for some regions – particularly the eastern subtropical Atlantic – but not for those boxes that include the Gulf Stream. Over the whole range considered, closure is obtained for 13 (9) out of 20 boxes with the NOC (NCEP/NCAR) surface fluxes. The seasonal heat budget at 20°–30° N, 35°–25° W is considered in detail. Here, the NCEP based budget has an annual mean residual of $-55\pm35\,\mathrm{W\,m^{-2}}$ compared with a NOC based value of $-4\pm35\,\mathrm{W\,m^{-2}}$. For this box, the net heat divergence of $36\,\mathrm{W\,m^{-2}}$ (Ekman=$-4\,\mathrm{W\,m^{-2}}$, geostrophic=$11\,\mathrm{W\,m^{-2}}$, diffusion=$29\,\mathrm{W\,m^{-2}}$) offsets the net heating of $32\,\mathrm{W\,m^{-2}}$ from the NOC surface heat fluxes. The results in this box are consistent with an earlier evaluation of the fluxes using measurements from research buoys in the subduction array which revealed biases in NCEP but good agreement of the buoy values with the NOC fields.

1 Introduction

Closure of the upper ocean heat budget has been a focus of many studies as it provides insights into the various processes controlling the temperature of the near surface layer and potentially places an important constraint on the air-sea heat exchange. Until recently, attempts to estimate the budget have been severely limited by lack of data. However, with the advent of the global array of Argo profiling floats (Gould, 2005) profiles of temperature are now routinely available on a regular basis to a maximum depth

of 2000 m over much of the global ocean.

In this paper we use the Argo data together with estimates of surface heat exchange from the NCEP/NCAR reanalysis (referred to as NCEP hereafter, Kalnay et al., 1996) and the NOC 1.1 surface flux dataset (NOC hereafter, Josey et al., 1999) to investigate the upper ocean heat budget in various regions of the North Atlantic. Gill and Niiler (1973) proposed and gave strong evidence for, the proposition that on a large scale (greater than 5° latitude by 5° longitude) the heat budget of the upper ocean is dominated by the local change in heat storage and surface heat fluxes, and that the advection and mixing terms are relatively small. However, in the North Atlantic advection by the meridional overturning circulation is a significant component of the heat budget. The northward heat flux at 26° N is about 1 PW (Bryden and Imawaki, 2001) which corresponds to a net annual heat flux from the ocean (26° to 70° N) to the atmosphere of $\sim 48\,\mathrm{W\,m^{-2}}$. This assumes that all the heat is released from the ocean between 26° N and 70° N and the surface area is $2.08\times10^{13}\,\mathrm{m^2}$. This flux can be compared with monthly heat fluxes of up to $\pm 500\,\mathrm{W\,m^{-2}}$. Though the advection and diffusion terms are smaller than the heat storage they still make a significant contribution to the monthly heat budget.

Here we evaluate the total heat budget, including each of the terms noted above, for the North Atlantic using data from the Argo profiling floats which provide continuous coverage from 1999–2005. To check on the validity of our approach an earlier analysis based on the Ocean Circulation and Climate Advanced Model (OCCAM, Webb et al., 1998), has been used to determine the Argo sampling error in monthly mixed layer heat storage estimates (Hadfield et al., 2007a). Using OCCAM sub-sampled at the Argo positions, it was found that the mixed layer monthly heat storage, in the subtropical North Atlantic but not including the Gulf Stream, has a sampling error of $10\text{–}20\,\mathrm{W\,m^{-2}}$ when averaged over a $10^\circ\times10^\circ$ area. This sampling error is sufficiently small to provide useful estimates of the heat budget over a significant fraction of the basin.

The paper is divided as follows: in Sect. 2 we discuss the method for estimation of the total heat budget. Details of the data required to make these estimates are given in

Sect. 3. In Sect. 4, we present and discuss the main results of our analysis including individual terms, the total heat budget and error estimates. Finally, we draw some conclusions in Sect. 5.

2 Heat budget method

The heat budget for the upper ocean is given by:

$$h\frac{\partial T_a}{\partial t}+h\upsilon_a\cdot\nabla T_a+\nabla\int_{-h}^{0}\hat{\upsilon}\hat{T}\,dz+(T_a-T_h)(w_{-h})+hk_{x,y}\cdot\nabla^2T_a+k_z\frac{\partial^2T}{\partial z^2}=\frac{Q-Q_{-h}}{\rho C_p} \quad (1)$$

where T is potential temperature, υ, horizontal velocity with (u, v) the eastward and northward components, respectively, w, vertical velocity, h, depth of the upper ocean, $k_{x,y}$, k_z, horizontal and vertical diffusion coefficients, ρC_p, specific heat capacity per unit volume (with C_p and ρ set to constants of $3986\,\mathrm{J\,kg^{-1}\,°C^{-1}}$ and $1027\,\mathrm{kg\,m^{-3}}$, respectively), Q, net absorbed surface heat flux $\mathrm{W\,m^{-2}}$, Q_{-h}, the penetrative solar radiation heat flux $\mathrm{Wm^{-2}}$, $\nabla\equiv(\partial/\partial x, \partial/\partial y)$ the horizontal gradient, x, y and z the eastward, northward and upward coordinates, respectively, and t, time. The subscripts h and a are used to indicate variables at depth h and averaged between depth h and the sea surface, respectively, $\hat{\upsilon}$ is the deviation from the vertically averaged velocity field ($\upsilon=\upsilon_a+\hat{\upsilon}$) and $\hat{T}$ is the deviation from the vertically averaged temperature ($T=T_a+\hat{T}$). This procedure is based on Stevenson and Niiler (1983) and adapted by Hadfield et al. (2007a).

The individual terms are: $h\frac{\partial T_a}{\partial t}$ is the local change in heat storage, $h\upsilon_a\cdot\nabla T_a$ is the horizontal advection of temperature, $\nabla\int_{-h}^{0}\hat{\upsilon}\hat{T}\,dz$ is the covariance of the horizontal velocity and temperature, $(T_a-T_h)(w_{-h})$ is the vertical advection of temperature at depth h, $hk_{x,y}\cdot\nabla^2T_a$ is the horizontal diffusion of temperature, $k_z\frac{\partial^2T}{\partial z^2}$ is the vertical diffusion of temperature, Q is the net downward heat flux at the sea surface and Q_{-h}, is the penetrative solar radiation at depth h. The two data sets used here for the net surface

heat flux are the National Oceanography Centre air-sea fluxes determined by Josey et al. (1998) and the National Centre for Environmental Prediction/National Centre for Atmospheric Research (NCEP/NCAR) reanalysis (Kalnay et al., 1996; Kistler et al., 2001).

The horizontal velocity (u, v) is partitioned into two components: the wind stress induced Ekman flow (u_e and v_e) and the geostrophic flow (u_g and v_g). The Ekman flow is given by:

$$u_e = \frac{\tau_y^0}{\rho_0 f h} \quad \text{and} \quad v_e = -\frac{\tau_x^0}{\rho_0 f h}$$

where (τ_x^0, τ_y^0) are components of wind stress, ρ_0=sea water density, h=mixed layer depth and f=coriolis parameter.

The surface wind stress is obtained from the NOC and NCEP wind stress values, and the mixed layer depth is defined as the depth at which the temperature is 0.2°C below the surface temperature. This definition allows capture of the spring re-stratification (Montegut et al., 2004). Argo floats only give reliable temperatures up to 10 m below the surface and therefore this is used as a surface temperature. The Ekman flow is assumed to be contained within the mixed layer. This may not always be the case, in particular, in the subtropical regions where Ekman flows can be deeper than the mixed layer and we make an estimate of this error (Sect. 4.3).

The geostrophic flow (u_g and v_g) is determined from the slope of sea level and a contribution from the density field within the upper ocean (0–300 m). Argo profiles are used to determine sea level height by the Bernoulli inverse method (Cunningham, 2000; Alderson and Killworth, 2005). In the method the three properties conserved along streamlines are the compressible Bernoulli function, salinity and the modified potential temperature. This modified potential temperature is a linear combination of potential heat content and salinity. The Bernoulli Inverse method provides a best estimate of sea level height together with an error estimate for the period January 2003 to December 2005 only. For the earlier period (January 1999 to December 2002),

sufficient salinity data was not available and therefore sea level height could not be determined. For this earlier period a temporal mean value from January 2003 to December 2005 is adopted. The baroclinic contribution to the geostrophic flow, was found to be small when compared with the barotropic contribution from the sea level slope.

The covariance of velocity and temperature ($\nabla \int_{-h}^{0} \hat{o}\hat{T}\,dz$) is ignored in this study. Estimates suggest that its contribution to the heat budget is much less than $5\,\mathrm{W\,m^{-2}}$ (Hadfield et al., 2007). The vertical velocity has two components (i) Ekman pumping velocity calculated from the wind stress curl $w_e = \frac{\nabla \wedge \tau^0}{\rho_0 f}$ of the NCEP/NCAR and NOC data sets and (ii) the geostrophic convergence ($w_g = -\frac{\beta v_g h}{f}$) associated with the change in Coriolis parameter with latitude, β. The vertical velocity w_g is calculated from the northward component of the geostrophic velocity, v_g, the depth h, and f the Coriolis parameter.

The horizontal diffusion coefficient is assumed to be $5000\,\mathrm{m^2\,s^{-1}}$ in all boxes. This value was adopted by McCulloch and Leach (1998) in their heat budget analysis of the North Atlantic. The value represents the horizontal eddy diffusivity estimated from buoys drogued at 100 m (Schafer and Kraus, 1995). This value is larger than that estimated by Ledwell et al. (1993) from the North Atlantic Tracer Release Experiment, who estimated values from 650 to $2300\,\mathrm{m^2\,s^{-1}}$ on scales from 300 km to 1000 km. The vertical mixing coefficient has a value of $2\times10^{-5}\,\mathrm{m^2\,s^{-1}}$ (Ledwell et al., 1993) and represents vertical mixing within the upper layer on horizontal scales of hundreds of kilometers and time scales of months.

3 Data objective analysis method

All the Argo profiles collected between 1 January 1999–31 December 2005 in the North Atlantic from 0° N to 70° N and 0°–100° W, and reaching a depth of at least 1000 m are used in this study. Argo floats are designed to sample an ocean area of 3°×3° resolution at a frequency of 10 days, however, the Argo array was significantly lower

than this resolution for large parts of the North Atlantic, particularly during the early years of Argo. This means that our choice of box size for the heat budget has to reflect this resolution for there to be sufficient samples. With the use of an eddy permitting ocean model (OCCAM) we have found (see Hadfield et al., 2007a) that a monthly time scale and a horizontal resolution of 10°×10° degree boxes, is sufficient to obtain good estimates of the terms in Eq. (1).

We adopted an objective analysis method (Gandin, 1963; Bretherton et al., 1976; Böhme and Send, 2005; Hadfield et al., 2007a) to obtain the best linear estimate of temperature at a given horizontal position and given vertical level. The method is discussed fully by Hadfield et al. (2007a) and here we will outline the basis of the method. In this study the covariance of the data is assumed to be Gaussian, with a decay scale determined by four correlation parameters: a longitudinal scale (Lx), a latitudinal scale (Ly), a cross-isobath scale (Φ), and a temporal scale (Δt). The objective estimate of the potential temperature at a grid point T_{grid} , for each 10 decibar level, is given by:

$$T_{\text{grid}} = T_{\text{WOA}} + \sum_{i=1}^{N} w_i (T_i - T_{\text{WOA}})$$

T_i denotes the "N" profiles closest in space and time to the grid point being interpolated to. It was found that beyond N=40 there was little discernible difference to the interpolated value, and therefore we set N=40 for this analysis.

T_{WOA} is the monthly mean field from the World Ocean Atlas (WOA) (Stephens et al., 2001) climatology. The weighting matrix **w** is given by $\mathbf{w}=\mathbf{Cdg}\bullet\mathbf{Cdd}^{-1}$ where **Cdg** is the covariance matrix between the analysed value at the observation point and the grid point value or the data-grid covariance. $\mathbf{Cdd}^{-1}$ is the inverted covariance matrix between observation points or the data-data covariance.

Given a very large number of observations randomly distributed over the North Atlantic we could evaluate **Cdd** directly. However, this is not the case, and we choose the following Gaussian model function to describe the covariance functions (Böhme and

Send, 2005). The data-grid covariance is:

$$\mathbf{Cdg}_i = \langle s^2 \rangle \cdot \exp\left\{ -\left[\frac{Dx_{i,g}^2}{Lx^2} + \frac{Dy_{i,g}^2}{Ly^2} + \frac{F_{i,g}^2}{\Phi^2} + \frac{Dt_{i,g}^2}{\Delta t^2} \right] \right\}$$

The data-data covariance is:

$$\mathbf{Cdd}_i = \langle s^2 \rangle \cdot \exp\left\{ -\left[\frac{Dx_{i,j}^2}{Lx^2} + \frac{Dy_{i,j}^2}{Ly^2} + \frac{F_{i,j}^2}{\Phi^2} + \frac{Dt_{i,j}^2}{\Delta t^2} \right] \right\}$$

Dx and Dy are the spatial distances between the floats and the grid point in the zonal and meridional directions, respectively, and Dt is temporal separation between the float and grid point. F, the cross isobath separation, is calculated from the following formula,

$$F = \frac{|\mathrm{PV}(a) - \mathrm{PV}(b)|}{\sqrt{\mathrm{PV}^2(a) + \mathrm{PV}^2(b)}}$$

where PV is the barotropic potential vorticity, f/H, f is the Coriolis parameter and H is the full ocean depth. The inclusion of the cross-isobath separation considers the tendency of ocean currents to follow the bathymetry. The subscripts refer to the grid point (g), the observation point (i) and another observation point (j). s^2 is the signal variance defined $s^2 = \frac{1}{N}\sum (T_i - T_{\mathrm{WOA}})^2$ where T_i is the float temperature and T_{WOA} is the climatogical temperature or the first guess field for optimal interpolation. N is the number of closest floats and here N=40.

The chosen values for Lx, Ly, Φ , and Δt, depend on the availability of observations. If there are too few observations then the interpolation will be strongly weighted to the climatology, whilst if there are too many observations there will be over-smoothing of the data. We choose a length scale of 500 km, time scale of 30 days and Φ=0.25 at the surface. The horizontal scale decreases linearly to 250 km at 500 m depth and the time scale increases linearly to 90 days. Below this the values remain constant.

The Argo temperature data were optimally interpolated onto monthly 2°×2° bins throughout the North Atlantic using the 40 closest Argo profiles to each grid point and the WOA (2001) climatology as the first guess field. By this method values of potential temperature were interpolated onto 104 horizontal surfaces (from 10 m, 15 m to 200 m, 210 m to 500 m, 520 m to 1000 m, 1050 m to 1500 m). The values were interpolated to the centre point of each calendar month from February 1999 to December 2005. The heat budget has been calculated using a fixed depth of 300 m, to calculate heat storage. The monthly interpolated fields were then averaged into 10°×10° bins for the heat budget analysis and a 3 monthly running mean was applied. These spatial and temporal scales were chosen in view of a model based analysis of error estimates in the heat budget terms; these scales represent the minimum scales which could be reliably resolved over large areas of the North Atlantic and for the majority of the study period (Hadfield et al., 2007a). Studies of the heat budget from 2006 onwards and in higher sampled regions of the North Atlantic may be possible at a higher resolution.

The 7 year mean seasonal cycle of the mixed layer depth (Fig. 1), shows that to the south of 50° N the maximum depth is less than 200 m at 10°×10° resolution. At the higher resolution 2°×2° the maximum mixed layer can exceed depths of 300 m locally near the Gulf Stream. In the northern most boxes (50°–60° N) the deepest mixed layers approach 300 m at this resolution. At higher resolution 2°×2°, mixed layers can approach 500 m depth in the Labrador Sea, Irminger Sea and Greenland Sea, however at this resolution there are insufficient Argo floats to provide a good estimate of the heat storage. Furthermore, as the depth of the chosen layer is increased, signals from the ocean interior tend to dominate over those in the upper ocean. The chosen depth of 300 m is therefore a compromise between the Argo sampling and the need to sample the upper ocean adequately at a 10°×10° resolution.

The mean seasonal cycle of the depth averaged temperature (0–300 m) T_a and the temperature at 300 m is shown in Fig. 2. T_a shows a seasonal cycle of about 1°C, whilst T_{-h} shows little seasonal variation. In the lowest latitudes (T_{-h} is significantly below T_a, because of the shallower mixed layer depths at these latitudes; Fig. 1). In the most

northern boxes T_a is close to T_{-h} in late winter, at the time of the deepest mixed layers.

4 Results

4.1 NCEP and NOC net heat flux fields

We first compare the NCEP and NOC net heat flux fields for the period January 1999 to December 2005. Annual mean values averaged onto 10×10° boxes are listed in Table 1 and the seasonal cycle for each box is shown in Fig. 3. The NCEP fields have greater heat loss (or weaker heat gain in summer) than NOC and this is consistent with previous studies which have found strong net heat loss values in the NCEP fields arising from the latent and sensible heat flux terms (Josey, 2001; Renfrew, 2002). In the annual mean, the differences are largest towards the western boundary at 30°–40° N with the NCEP net heat loss exceeding NOC by up to 47 W m^{-2}. Closer agreement is found elsewhere, with the lowest RMS differences (<20 W m^{-2}) in the eastern basin at 40°–50 ° N.

Given the RMS results we expect a close correspondence between the NOC and NCEP seasonal cycles of net heat flux in the eastern basin at 40°–50° N and this is found to be the case (Fig. 3). Further south, an offset is introduced between the two seasonal cycles with NCEP persistently lower than NOC in the range 20°–30° N. Note that in the eastern part of this range the NOC net heat flux has previously been shown to be in good agreement with high quality measurements from WHOI flux buoys deployed as part of a subduction study (Josey, 2001). Finally, note that the largest differences between NCEP and NOC in the annual mean towards the western boundary at 30°–40° N, commented on above, are primarily the result of stronger NCEP heat loss in the winter months.

4.2 Heat storage

Annual mean heat storage values have been determined for the full period 1999–2005 (Table 2) and these indicate that the heat storage change is not significantly different from zero within the error of the estimate for all boxes. This is to be expected if there is no significant change in temperature over this period. Note that the heat storage errors are smallest in the eastern and central subtropical gyre (30°–40° N, 15°–45° W), and greatest in the Gulf stream extension region (40°–50° N, 45°–65° W).

The monthly change in heat storage, $\rho C_p h \frac{\partial T_a}{\partial t}$ from Eq. (1), is shown in Fig. 4 with estimated errors for each of the 10°×10° boxes. The errors exceed 100 W m^{-2} in the Gulf Stream (40°–50° N, 45°–65° W), but decrease markedly away from this region. The maximum rate of change is generally associated with the winter and summer solstice in December and June, except for the region (30°–40° N, 45°–65° W) where the maximum is delayed by one month. The zero change in heat storage occurs in March when the minimum heat storage is found, and September when the maximum heat storage occurs.

The error ranges shown on the figure are due to spatial and temporal undersampling and have been determined by sub-sampling the OCCAM model using the temporal and spatial positions of the Argo floats. The RMS differences between the fully sampled model heat storage and the sub-sampled heat storage provided an estimate of the sampling error. Note that instrument errors have been largely removed by a range of quality control procedures (see Hadfield et al., 2007a.). The errors sampling are largest at 40°–50° N, west of 45° W in the region of the Gulf Stream extension. They are also large in the upwelling region off the N. W. African Coast (30°–40° N, 5°–15° W). The large values for the errors are associated with the high spatial gradients and temporal variability in these regions where major contributions by advection and diffusion are expected.

The mean monthly change in heat storage is compared with the NCEP and NOC fluxes in Fig. 5. Good correspondence with both NCEP and NOC fluxes is found in

OSD
6, 95–128, 2009

many of the southern and eastern regions of the North Atlantic. In particular, for all 6 of the 20°–30° boxes, four of the 30°–40° boxes, and 2 of the 40°–50° boxes, the heat storage estimates are close to or within the estimates of the two surface heat flux datasets. The boxes west of 45° W between 30° N and 40° N, and west of 25° W between 40° N and 50° N, which contain the Gulf Stream extension and the North Atlantic Current, have much larger seasonal heat storage cycles than can be accounted for by surface heat flux variations alone. The enhancement of the heat storage is probably related to advection and mixing processes within the ocean and this is discussed in Sect. 4.3.

4.3 Heat advection and diffusion

In order to understand the relationship between the heat storage and the surface fluxes it is necessary to consider all the terms in the heat budget from 0–300 m described in Eq. (1) and we now consider the contributions due to advection and diffusion. The annual mean Ekman contribution to the horizontal heat divergence is shown in Fig. 6 and Table 3 for NCEP and NOC wind stress values, respectively, together with error estimates. Both the NCEP and NOC wind stress estimates and heat divergences are very similar on this scale. Positive values of heat divergence (cooling) occur between 30° N and 60° N, with large values of up to 28 W m^{-2} at about 50° N close to the position of the Gulf Stream extension and the North Atlantic current. This region is associated with enhanced westerly wind stress and large horizontal temperature gradients. Heat convergence (warming) is generally confined to lower latitudes below 20° N. This is associated with the easterly trade winds enhancing the Ekman flux towards the centre of the subtropical gyre, and hence exporting heat into this region. The exception to this is the upwelling area off North Africa, where heat divergence is found. There is a strong seasonal variation in the Ekman contribution (Fig. 7) with largest values during the winter period up to ~50 W m^{-2} east of Newfoundland (45°–55° W, 40°–50° N box). Estimates of error associated with the penetration of the Ekman layer below the mixed layer are −4 to 7 W m^{-2} with an average RMS error of 0.9 W m^{-2}.

The geostrophic heat divergence (Table 4) has values ranging from zero to more

than 150 W m^{-2} east of Newfoundland and with a standard deviation of 40 W m^{-2}. The errors for the geostrophic divergence come mainly from the estimate of the sea level pressure gradient obtained from the Bernoulli method and the Argo hydrographic profiles. There is little seasonal signal in the geostrophic heat divergence, despite the seasonal variability in wind stress and Ekman transport.

The final contribution to the heat budget comes from the diffusion terms. Table 5 and Fig. 8 show the annual mean heat divergence from diffusion, and the seasonal cycle, respectively. The annual mean values range from 4 to 76 W m^{-2} with the largest values at 30°–40° N, 45°–55° W (east of Newfoundland). These calculated values are based on a horizontal coefficient typical of the North Atlantic at this scale in the upper 100 m, but the uncertainty of this coefficient is high close to the Gulf Stream extension region and consequently the estimated errors are large. The errors in the diffusion term are difficult to estimate and are assumed to be 100% of the calculated value. With this assumption, the errors are greatest in the Gulf Stream where both horizontal and vertical diffusion terms make a significant contribution to the heat budget. The smallest contribution is in the eastern subtropical Atlantic where the horizontal temperature gradients are weakest.

We have combined the individual sources of error discussed above, assuming that they are independent, to give an overall estimate of error in the residual heat budget shown in Table 6 and this will be discussed in the next section.

4.4 Closing the heat budget

We now consider the extent to which the heat budget can be closed for individual 10×10 degree boxes in the North Atlantic. The residual (R) is defined to be sum of the individual terms in Eq. (1) (i.e. R=Surface Flux−Change in Heat Storage−Advection−Diffusion). a positive value of the Residual indicates the heat budget has an excess of heat into the ocean. When R is less than the overall estimated error the heat budget is said to be closed. The residual therefore provides a measure

of the closure of heat budget using either the NCEP or the NOC fluxes. First, the seasonal heat budget for two specific boxes will be presented, followed by a more the general discussion of the residuals for all of the boxes in the 20°–60° N latitude range.

Figure 9 shows the components of the heat budget for a box at 20°–30° N, 35°–25° W, in the subtropical Atlantic Ocean, where the residual heat flux is small. The budget has been determined for surface heat fluxes from NCEP (red) and NOC (blue). The correspondence between the heat storage (green) and the surface fluxes is reasonably good. The heat storage lies within the envelope of NOC and NCEP, and whilst the agreement is better with NCEP in the early half of year, with NCEP it is poorer in late summer and autumn. The residual of the heat budget shows that over the year the use of the NOC flux brings the budget closer to zero than when NCEP is used. The NCEP budget has an annual mean residual of $-55\pm35\,\mathrm{W\,m^{-2}}$ compared with a NOC value of $-4\pm35\,\mathrm{W\,m^{-2}}$. At this box we find that the net heat divergence of $36\,\mathrm{W\,m^{-2}}$ (Ekman$=-4\,\mathrm{W\,m^{-2}}$, geostrophic$=11\,\mathrm{W\,m^{-2}}$, diffusion$=29\,\mathrm{W\,m^{-2}}$) offsets the net heating from the NOC surface heat fluxes.

a second example of the heat budget is given at 40°–50° N, 25°–15° W (Fig. 10). The heat budget for this box is dominated by surface heat flux and heat storage and heat convergence makes only a small contribution. The residual is less than the error estimate for both NCEP ($-4\pm12\,\mathrm{W\,m^{-2}}$) and NOC ($+7\pm12\,\mathrm{W\,m^{-2}}$) and therefore confirms the closure for this box to this accuracy. However, we cannot distinguish any difference in residual when NCEP and NOC net surface fluxes are used in the heat budget.

The values of the residuals for all of the individual boxes are shown in Fig. 11 and Table 6. For the latitude band 20°–30° N, the NOC fluxes produce closure in 5 of the 6 boxes, whilst for NCEP fluxes closure is found in 3 of the 6 boxes. In the range 30°–40° N there is closure in only one NCEP box, whilst NOC has closure in 2 of the 5 boxes. Further north, for 40°–50° N closure is obtained for 2 boxes using NCEP and NOC. Finally, at 50°–60° N we have closure of all 4 of the NOC boxes and 3 of the NCEP boxes. Over the whole range 20°–60° N, closure is obtained for 13 (9) out of 20 boxes with NOC (NCEP) surface fluxes.

5 Summary and conclusion

An analysis of the heat budget of the upper ocean (0–300 m) for the North Atlantic from 20°–60° N based on Argo profiling floats and surface flux fields from NCEP/NCAR and NOC has been presented. Individual terms in the budget have been assessed for 10°×10° boxes in the North Atlantic and closure of the heat budget is obtained within the error estimates for some regions but not for those boxes that include the Gulf Stream. For NCEP, 9 out of 20 boxes, and for NOC, 13 out of 20 boxes meet the criterion of closure within the estimated error.

The lowest error estimates for the net heat budget ($\pm 9\,\mathrm{W\,m^{-2}}$) are in the eastern and central subtropical gyre for two boxes 35°–25° W and 25°–15° W between 30° N and 40° N.

The analysis of the 35°–25° W box has shown that closure of the heat budget can be obtained with both NCEP and NOC surface fluxes. Further south, a detailed seasonal heat budget for the box (20°–30° N, 35°–25° W) reveals a large residual in the heat budget when NCEP is used $-55\pm35\,\mathrm{W\,m^{-2}}$ whilst when NOC fluxes are applied the residual is small $-4\pm35\,\mathrm{W\,m^{-2}}$. This is consistent with an earlier evaluation of the NOC and NCEP/NCAR fluxes using measurements from research buoys in the subduction array (Moyer and Weller, 1997; Josey, 2001) which revealed biases in NCEP but good agreement of the buoy values with the NOC fields (Josey, 2001).

To conclude, closure of the heat budget using Argo data combined with surface flux fields has been obtained for 65% of the 10×10 degree boxes considered in the North Atlantic when NOC surface heat fluxes have been used and 45% when NCEP fluxes are used. Significant problems remain at present towards the western boundary region including the Gulf Stream where closure has not been achieved. Our analysis has only considered Argo data up to the end of 2005 and the region 20°–60° N. As the time period covered by Argo and number of floats increases, we anticipate being able to obtain a better understanding of the processes controlling the heat budget over a greater region of the Atlantic and other ocean basins.

OSD
6, 95–128, 2009

References

Alderson, S. G. and Killworth, P. D.: a preoperational scheme for calculating sea surface height by Bernoulli inverse of Argo float data in the North Atlantic, J. Atmos. Ocean. Tech., 22(9), 1416–1422, 2005.

Böhme, L. and Send, U.: Objective analyses of hydrographic data for referencing profiling float salinities in highly variable environments, Deep-Sea Res. Pt. II, 52(3–4), 651–664, 2005.

Bretherton, F. P., Davis, R. E., and Fandry, C. B.: a technique for objective analysis and design of oceanographic experiments applies to MODE-73, Deep-Sea Res., 23, 559–582, 1976.

Bryden, H. L. and Imawaki, S.: Ocean heat transport, in: Ocean Circulation and Climate, edited by: Seidler, G., Church, J., and Gould, J., Academic Press, 455–474, p. 715, 2001.

Cunningham, S. A.: Circulation and volume flux of the North Atlantic using synoptic hydrographic data in a Bernoulli inverse. J. Mar. Res., 58(1), 1–35, 2000.

Gandin, L. S.: Objective Analysis of Meteorological Fields, Gidrometeorol Izdat, Leningrad, 242 pp., 1963.

Gill, A. E. and Niiler, P. P.: The theory of seasonal variability in the ocean, Deep-Sea Res., 20, 141–177, 1973.

Gould, W. J.: From Swallow floats to Argo-the development of neutrally buoyant floats, Deep-Sea Res. Pt. II, 52, 529–543, 2005.

Hadfield, R. E., Wells, N. C., Josey, S. A., and Hirschi, J. J.-M.: On the accuracy of North Atlantic temperature and heat storage fields from Argo, J. Geophys. Res., 112, C01009, doi:10.1029/2006JC003825, 2007a.

Hadfield, R. E.: The North Atlantic study: an Argo based study, Ph.D. thesis, University of Southampton, 198 pp., 2007b.

Josey, S. A., Kent, E. C., and Taylor, P. K.: The Southampton Oceanography Centre (SOC) ocean-atmosphere heat, momentum, and freshwater flux atlas, National Oceanography Centre, Southampton, UK, Southampton report 6, 30 pp., 1998.

Josey, S. A., Kent, E. C., and Taylor, P. K.: New insights into the ocean heat budget closure problem from analysis of the SOC air-sea flux climatology, J. Climate, 12(9), 2856–2880, 1999.

Josey, S. A.: a comparison of ECMWF, NCEP-NCAR and SOC surface fluxes with moored buoy measurements in the subduction region of the Northeast Atlantic, J. Climate, 14, 1780–1789, 2001.

Kalnay, E., Kanamitsu M., Kistler R., et al.: The NCEP/NCAR 40 year reanalysis project, B. Am. Meteorol. Soc., 77, 437–471, 1996.
Kistler, R., Kalnay, E., Collins, W., et al.: The NCEP/NCAR 50 year reanalysis project: monthly means and CD-ROM and documentation, B. Am. Meteorol. Soc., 82(2), 247–267, 2001.
Ledwell, J. R., Watson, A. J., and Law, C. S.: Evidence for slow mixing across the pycnocline from an open-ocean tracer release experiment, Nature, 364(6439), 701–703, 1993.
McCulloch, M. E. and Leach, H.: Air-sea fluxes inferred from an upper ocean heat budget north east of the Azores, Q. J. Roy. Meteor. Soc. 124, 2465–2476, 1998.
Montegut, C. D. et al.: Mixed layer depth over the global ocean: an examination of profile data and profile based climatology, J. Geophys. Res., 109, C12003, doi:10.1029/2004JC002378, 2004.
Moyer, K. A. and Weller, R. A.: Observations of surface forcing from the Subduction Experiment: a comparison with global model products and climatological data sets, J. Climate, 10, 2725–2742, 1997.
Renfrew, I. A., Guest, P. S., and Bumke, K.: a comparison of surface layer and surface turbulent flux observations over the Labrador Sea with ECMWF analyses and NCEP analyses, J. Phys. Oceanogr., 32, 383–400, 2002.
Schafer, H. and Kraus, W.: Eddy statistics in the South Atlantic as derived from drifters drogued at 100 m, J. Mar. Res., 53, 403–431, 1995.
Stephens, C., Antonov, J. I., Boyer, T. P., Conkright, M. E., Locarnini, R. A., O'Brien, T. D., Garcia, H. E., and Levitus, S.: World Ocean Atlas 2001, Volume 1: Temperature, NOAA atlas NESDIS 49, 176 pp., 2001.
Stevenson, J. W. and Niiler, P. P.: Upper ocean heat budget during the Hawaii-to-Tahiti Shuttle Experiment, J. Phys. Oceanogr., 13, 1895–1907, 1983.
Webb, D. J., de Cuevas, B. A., and Coward, A. C.: The first main run of the OCCAM global ocean model, Southampton Oceanography Centre, UK, Internal document 34, 44 pp., 1998.

Table 1. Annual mean net heat flux for a) NCEP and NOC, with the latter shown in brackets and b) the RMS difference between the two flux fields. Positive values indicate heat flux into the ocean.

a)	75°–65° W	65°–55° W	55°–45° W	45°–35° W	35°–25° W	25°–15° W	15°–5° W
50°–60° N	–	–	−19 (−10)	−27 (−27)	−33 (−23)	−50 (−29)	−36 (−18)
40°–50° N	–	−20 (−12)	−7 (6)	−84 (−54)	−29 (−15)	−11 (0)	−5 (11)
30°–40° N	−113 (−73)	−104 (−57)	−56 (−14)	−21 (12)	−1 (23)	−2 (13)	3 (30)
20°–30° N	−23 (22)	−19 (29)	−13 (35)	−10 (39)	−16 (36)	12 (42)	–
b)	75°–65° W	65°–55° W	55°–45° W	45°–35° W	35°–25° W	25°–15° W	15°–5° W
50°–60° N	–	–	23	19	26	30	27
40°–50° N	–	14	24	35	8	14	18
30°–40° N	43	48	43	34	25	17	29
20°–30° N	45	49	48	50	52	29	–

Table 2. Annual mean values of fixed depth heat storage with error estimates, W m^{-2}.

	75°–65° W	65°–55° W	55°–45° W	45°–35° W	35°–25° W	25°–15° W	15°–5° W
50°–60° N	–	–	3±17	2±41	5±34	2±16	0±20
40°–50° N	–	−18±117	−5±104	−1±38	8±24	0±9	0±18
30°–40° N	1±44	−6±17	1±19	2±6	1±7	1±7	0±53
20°–30° N	0±16	0±19	3±26	1±9	3±18	−1±30	–

Table 3. Annual mean wind-driven heat convergence for individual 10°×10° boxes in the North Atlantic based on the NCEP reanalysis wind stress and the NOC climatology wind stress, with the latter given in brackets. Values are in W m^{-2}.

	75°–65° W	65°–55° W	55°–45° W	45°–35° W	35°–25° W	25°–15° W	15°–5° W
50°–60° N	–	–	1 (1)	12 (9)	15 (11)	9 (8)	3 (4)
40°–50° N	–	–	28 (29)	28 (26)	16 (13)	9 (8)	4 (4)
30°–40° N	3 (4)	5 (7)	4 (6)	3 (4)	2 (2)	2 (2)	1 (0)
20°–30° N	−6 (−8)	−6 (−7)	−6 (−7)	−5 (−5)	−4 (−4)	3 (4)	–

Table 4. Annual mean geostrophic heat convergence for individual 10°×10° boxes in the North Atlantic, W m^{-2}. Negative values indicate a warming contribution.

	75°–65° W	65°–55° W	55°–45° W	45°–35° W	35°–25° W	25°–15° W	15°–5° W
50°–60° N	–	–	3±2	22±10	−8±9	42±7	–
40°–50° N	–	–	−161±41	3±16	−24±6	−21±2	−10±2
30°–40° N	60±16	−9±4	−6±3	2±3	0±2	6±2	–
20°–30° N	13±2	−9±2	8±2	27±4	11±4	5±6	–

Table 5. The mean diffusive heat convergence for 10°×10° boxes in the North Atlantic.

	75°–65° W	65°–55° W	55°–45° W	45°–35° W	35°–25° W	25°–15° W	15°–5° W
50°–60° N	–	–	−55	−24	−16	27	47
40°–50° N	–	19	−76	34	17	5	−3
30°–40° N	–	29	35	22	4	4	4
20°–30° N	10	9	15	21	29	22	–

Table 6. The annual mean heat budget residual, ($W\,m^{-2}$) based on a) NCEP and b) NOC atmospheric variables. Bold text indicates where closure of the heat budget is obtained to within the quoted error (i.e. residual not significantly different from zero).

a)	75°–65° W	65°–55° W	55°–45° W	45°–35° W	35°–25° W	25°–15° W	15°–5° W
50°–60° N	–	–	**30±57**	**−29±55**	**−29±40**	−46±32	–
40°–50° N	–	–	206±136	−148±55	−47±32	**−4±12**	**3±18**
30°–40° N	–	−128±34	−89±40	−49±23	**−8±9**	−15±9	–
20°–30° N	−40±20	**−13±22**	**−32±31**	−54±24	−55±35	**−16±38**	–
b)	75–65° W	65–55° W	55–45° W	45–35° W	35–25° W	25–15° W	15–5° W
50°–60° N	–	–	**40±57**	**−26±55**	**−14±40**	**−25±32**	–
40°–50° N	–	–	219±136	−116±55	**−29±32**	**7±12**	20±18
30°–40° N	–	−78±34	−49±40	**−17±23**	17±9	**0±9**	–
20°–30° N	**7±20**	36±22	**16±31**	**−5±24**	**−4±35**	**12±38**	

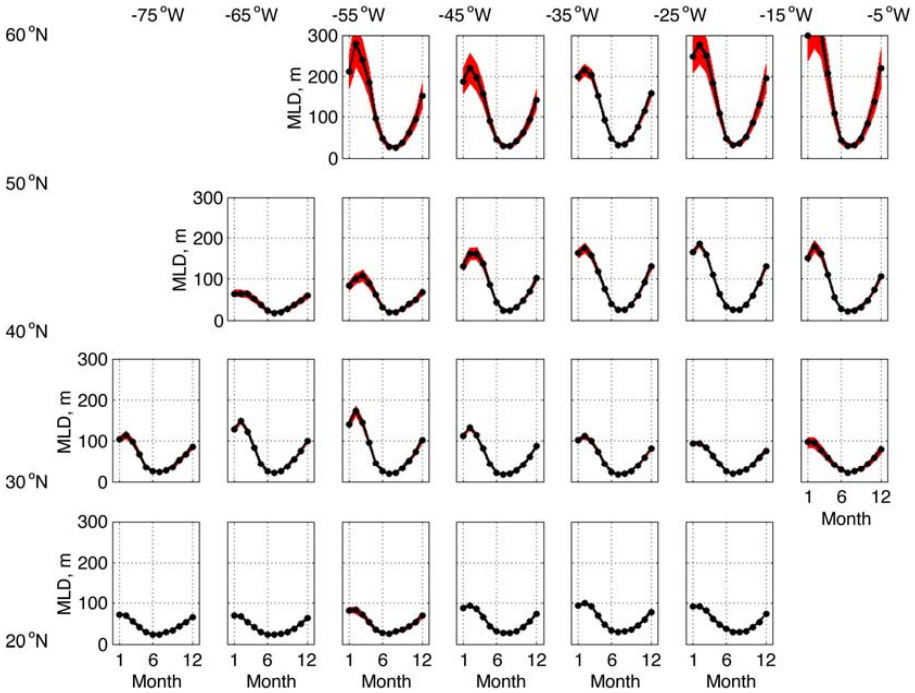

Fig. 1. Seasonal cycle in Mixed Layer Depth (m) for different 10°×10° boxes throughout the North Atlantic. The red shading indicates the estimated error.

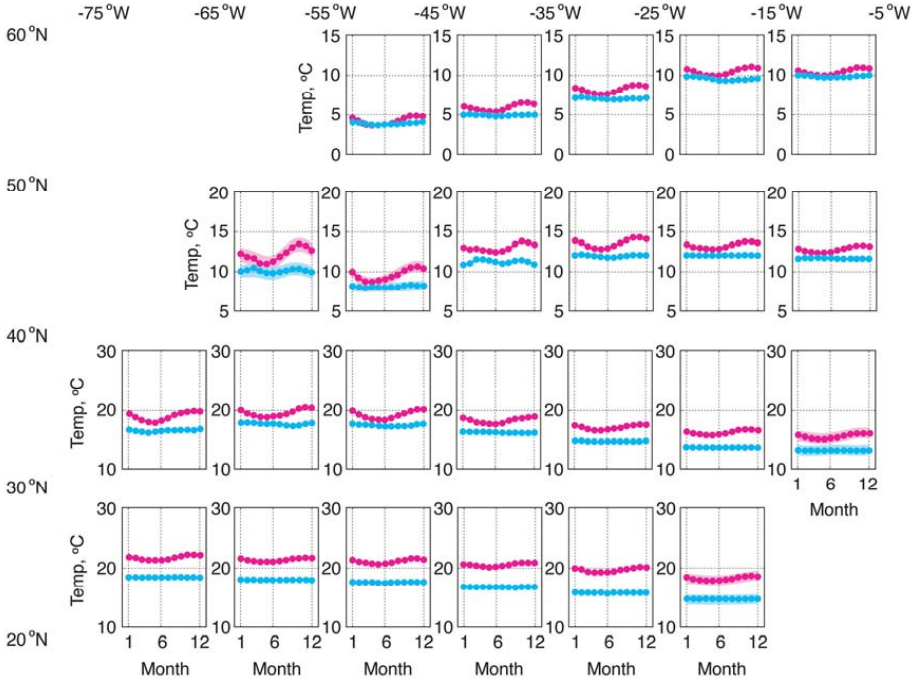

Fig. 2. Seasonal cycle in T_a over the upper 300 m (magenta) and $T_{-300\,m}$ (cyan) for different 10°×10° boxes in the North Atlantic. The shading indicates the errors associated with estimating the temperature variables from the Argo dataset.

OSD
6, 95–128, 2009

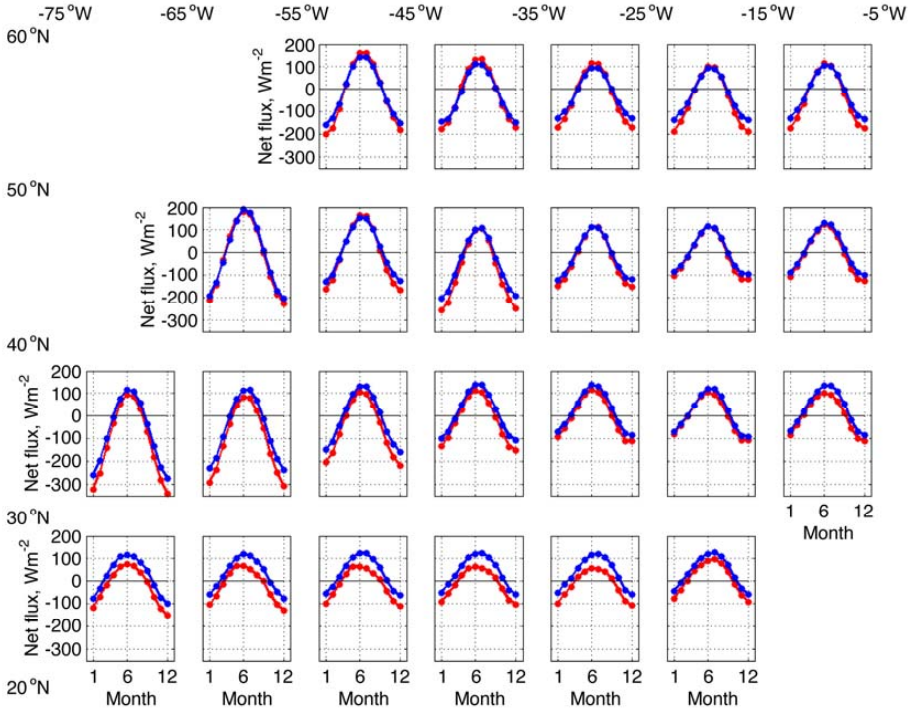

Fig. 3. Seasonal cycle in absorbed net flux for NCEP (red) and NOC (blue) derived using monthly averages between 1999 and 2005, values in W m^{-2}.

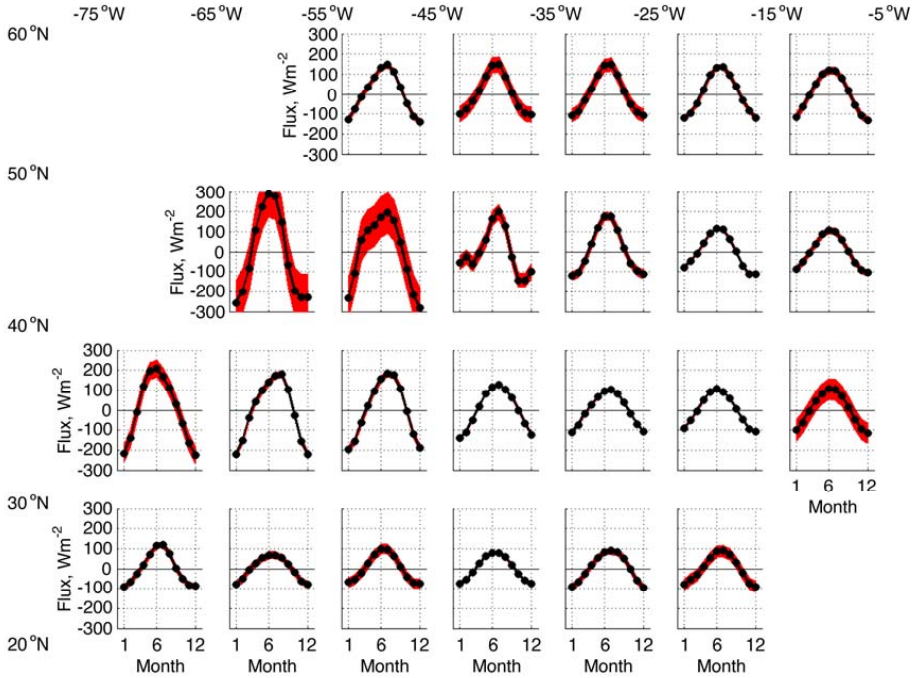

Fig. 4. Seasonal cycle in the heat storage of the upper 300 m ($W\,m^{-2}$) for different $10^{\circ} \times 10^{\circ}$ boxes in the North Atlantic. Red shading indicates the estimated error.

OSD
6, 95–128, 2009

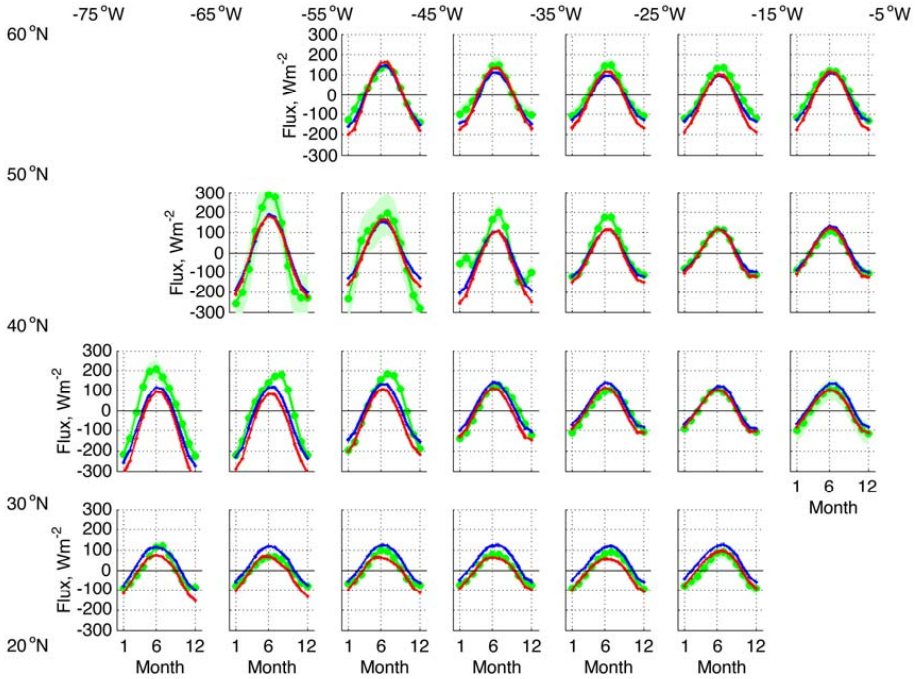

Fig. 5. Seasonal cycle in heat storage (green), absorbed net flux for NCEP (red) and NOC (blue) derived using monthly averages between 1999 and 2005, values in W m^{-2}.

OSD
6, 95–128, 2009

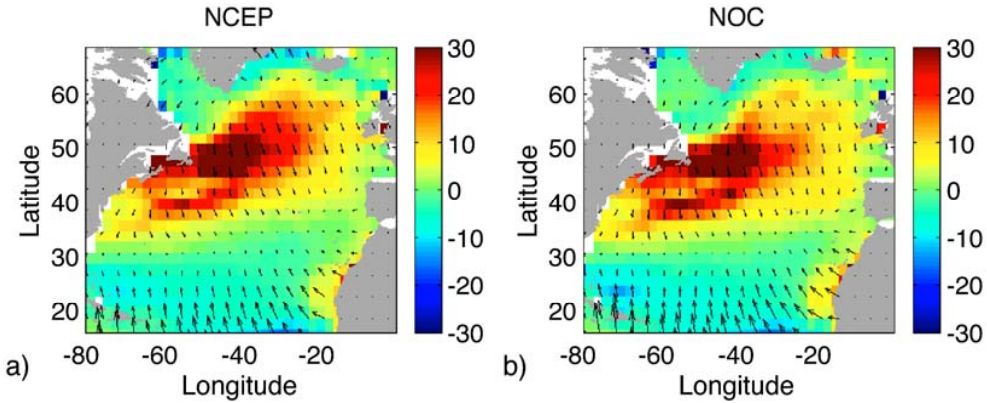

Fig. 6. The mean horizontal Ekman heat divergence calculated using **(a)** the NCEP wind stress field and **(b)** the NOC wind stress ($W\,m^{-2}$). Vectors indicate the direction of Ekman volume flux.

OSD
6, 95–128, 2009

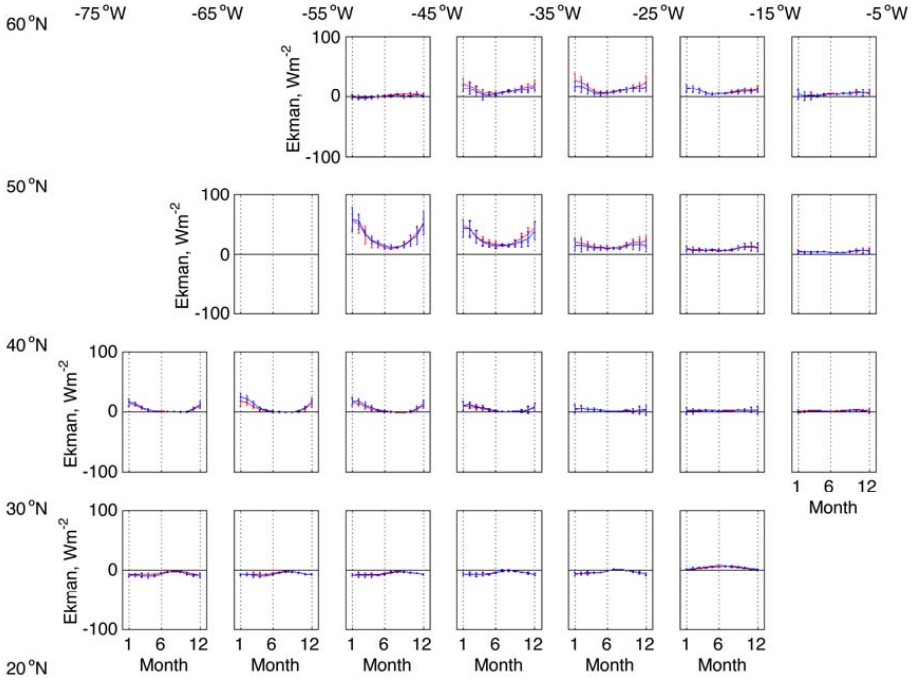

Fig. 7. Seasonal cycle in the horizontal Ekman heat convergence for different 10°×10° boxes in the North Atlantic. Fluxes based on the NCEP (red) and NOC (blue) wind stress fields are shown. The error bars indicate two standard errors of the seasonal values used to obtain the seasonal mean.

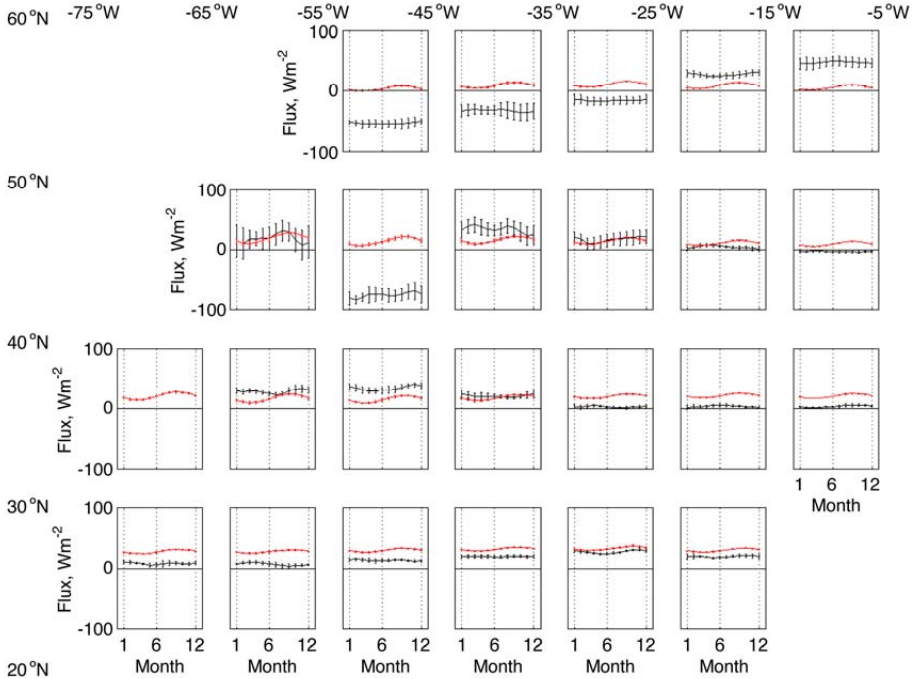

Fig. 8. Seasonal cycle in the diffusive heat flux for different 10°×10° boxes in the North Atlantic ($W\,m^{-2}$). Horizontal diffusion (black) and vertical diffusion (red) are shown separately. The error bars indicate two standard errors of the seasonal values used to obtain the seasonal mean.

OSD
6, 95–128, 2009

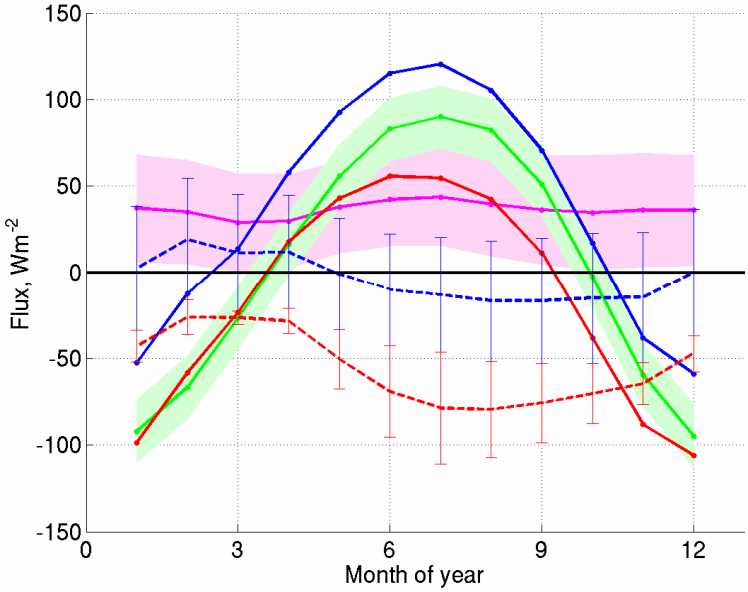

Fig. 9. The seasonal cycle in the heat budget components at 20°–30° N, 35°–25° W. The NCEP net heat flux (red), NOC net heat flux (blue), heat storage (green), heat convergence (pink), the NCEP heat budget residual (red dashed) and the NOC heat budget residual (blue dashed) are shown. Shading indicates estimated errors for each term.

OSD
6, 95–128, 2009

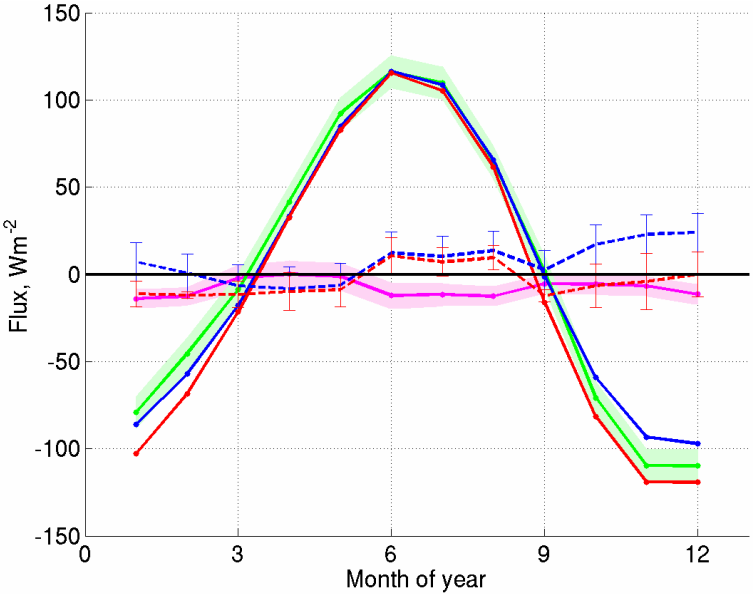

Fig. 10. The seasonal cycle in the heat budget components at 40°–50° N, 25°–15° W. The NCEP net heat flux (red), NOC net heat flux (blue), heat storage (green), heat convergence (pink), the NCEP heat budget residual (red dashed) and the NOC heat budget residual (blue dashed) are shown. Shading indicates estimated errors for each term.

OSD
6, 95–128, 2009

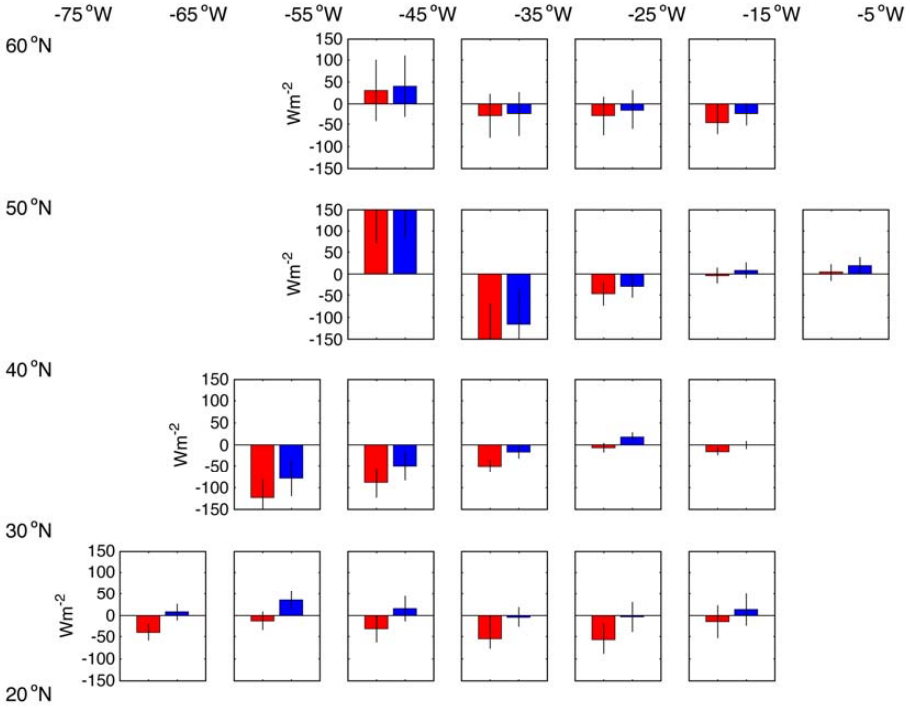

Fig. 11. Graphical representation of residual heat flux (see text for details). NCEP-based heat budget residual in red, NOC-based values in blue.